THE JOURNAL OF BIOLOGICAL CHEMISTRY VOL. 281, NO. 13, pp. 8981–8990, March 31, 2006

Crystallographic Evidence That the Dinuclear Copper Center of Tyrosinase Is Flexible during Catalysis*

Received for publication, September 6, 2005, and in revised form, December 29, 2005 Published, JBC Papers in Press, January 25, 2006, DOI 10.1074/jbc.M509785200

Yasuyuki Matoba[‡], **Takanori Kumagai**[‡], **Aiko Yamamoto**[‡], **Hironari Yoshitsu**[‡], **and Masanori Sugiyama**[‡§1]

From the [‡]*Department of Molecular Microbiology and Biotechnology, Graduate School of Biomedical Sciences and the* [§]*Frontier Center for Microbiology, Hiroshima University, Kasumi 1-2-3, Minami-ku, Hiroshima 734-8551, Japan*

At high resolution, we determined the crystal structures of copper-bound and metal-free tyrosinase in a complex with ORF378 designated as a "caddie" protein because it assists with transportation of two Cu(II) ions into the tyrosinase catalytic center. These structures suggest that the caddie protein covers the hydrophobic molecular surface of tyrosinase and interferes with the binding of a substrate tyrosine to the catalytic site of tyrosinase. The caddie protein, which consists of one six-stranded β-sheet and one α-helix, has no similarity with all proteins deposited into the Protein Data Bank. Although tyrosinase and catechol oxidase are classified into the type 3 copper protein family, the latter enzyme lacks monooxygenase activity. The difference in catalytic activity is based on the structural observations that a large vacant space is present just above the active center of tyrosinase and that one of the six His ligands for the two copper ions is highly flexible. These structural characteristics of tyrosinase suggest that, in the reaction that catalyzes the *ortho*-hydroxylation of monophenol, one of the two Cu(II) ions is coordinated by the peroxide-originated oxygen bound to the substrate. Our crystallographic study shows evidence that the tyrosinase active center formed by dinuclear coppers is flexible during catalysis.

Tyrosinase (EC 1.14.18.1), which belongs to a protein family having the catalytic center formed by dinuclear copper, catalyzes the *ortho*-hydroxylation of monophenol and the subsequent oxidation of the diphenolic product to the resulting quinone (1). A series of reactions occurs under the concomitant reduction of molecular oxygen to water. The quinone product is a reactive precursor for the synthesis of melanin pigments. Tyrosinase, which is contained in vegetables, fruits, and mushrooms, is a key enzyme in the browning that occurs upon bruising or long term storage. In mammals, the enzyme is responsible for skin pigmentation abnormalities, such as flecks and defects (2). Recently, the enzyme was reported to be linked to Parkinson disease and other neurodegenerative diseases (3, 4). Thus, tyrosinase is quite significant in the fields of medicine, agriculture, and industry. In the cosmetic industry, the development and screening of potent inhibitors of tyrosinase are especially attractive. However, the determination of the three-dimensional structure of tyrosinase has never been accomplished until now.

Tyrosinase is classified into the type 3 copper protein family, as are catechol oxidase and the respiratory pigment hemocyanin. During the catalytic reaction, the type 3 copper center of tyrosinase exists in three redox forms (1). The deoxy form [Cu(I)-Cu(I)] is a reduced species, which binds oxygen to give the oxy form [Cu(II)-O_2^{2-}-Cu(II)]. In the oxy form, molecular oxygen is bound as peroxide in a μ-η^2:η^2 side-on bridging mode, which destabilizes the O–O bond and activates it. The met form [Cu(II)-Cu(II)] is assumed as a resting enzymatic form, where Cu(II) ions are normally bridged to a small ligand, such as a water molecule or hydroxide ion.

Catechol oxidase oxidizes *ortho*-diphenols to the corresponding quinones but lacks monooxygenase activity. Hemocyanin acts as an oxygen carrier in arthropods and mollusks. Because the crystal structure of tyrosinase has been undetermined until now, the catalytic mechanism at the atomic level has not yet been elucidated. To build structural models of tyrosinase, it would be practical to reference the structural information from the type 3 copper protein members (5–11). As a common feature in the active site of these structures, each of two closely spaced copper ions is coordinated by three His residues through Nϵ nitrogen atoms. Although the active centers of the type 3 proteins are similar in both their overall structure and their ability to bind to molecular oxygen, their enzymatic functions differ. This is believed to result from a variation in the substrate-binding pocket or the accessibility of the substrate to the active site.

Many bacteria in the genus *Streptomyces* produce a melanin-like pigment (12–17). We have cloned a melanin-synthesizing gene from *Streptomyces castaneoglobisporus* HUT 6202, which forms an operon composed of two cistrons (12, 13): an open reading frame (ORF)[2] consisting of 378 nucleotides, designated *orf378*, was located just upstream of the tyrosinase gene designated *tyrC*. An ORF378-like protein, for example, ORF438 in *Streptomyces antibioticus*, is commonly present in some *Streptomyces* strains, and it has been suggested that it acts as a Cu(II)-carrier protein (18, 19). In fact, when the *S. castaneoglobisporus* tyrosinase is overexpressed using an *Escherichia coli* host-vector system (20), the coexpression of ORF378 is indispensable to obtain tyrosinase that has catalytic activity; the transport of Cu(II) ions to the catalytic center of tyrosinase, which is mediated by ORF378, may be necessary to convert tyrosinase to its active form. In the present study, we call ORF378 a "caddie" protein because it carries cupric ions for tyrosinase.

To study tyrosinase crystallographically, much effort was given to achieving the crystallization of the active tyrosinase; however, as a result of the high hydrophobicity of tyrosinase, the crystallization has never been successful. In fact, the crystallization of membrane proteins, which are difficult to dissolve at high concentration, has been unsuccessful without the help of an antibody specific to the protein (21–24). In the

* This work was supported by funds from the National Project on Protein Structural and Functional Analyses, Japan (to M. S.) and Hiroshima Biocluster (Cooperative Link of Unique Science and Technology for Economy Revitalization), Japan (to M. S.) and a Grant-in-Aid for Scientific Research from the Ministry of Education, Science, and Culture of Japan (to Y. M.). The costs of publication of this article were defrayed in part by the payment of page charges. This article must therefore be hereby marked "*advertisement*" in accordance with 18 U.S.C. Section 1734 solely to indicate this fact.

The atomic coordinates and structure factors (code 1WX5, 1WXC, 1WX3, 2AHK, 2AHL, and 1WX2) have been deposited in the Protein Data Bank, Research Collaboratory for Structural Bioinformatics, Rutgers University, New Brunswick, NJ (http://www.rcsb.org/).

[1] To whom correspondence should be addressed: Dept. of Molecular Microbiology and Biotechnology, Graduate School of Biomedical Sciences, Hiroshima University, Kasumi 1-2-3, Minami-ku, Hiroshima 734-8551, Japan. Tel.: 81-82-257-5280; Fax: 81-82-257-5284; E-Mail: sugi@hiroshima-u.ac.jp.

[2] The abbreviation used is: ORF, open reading frame.

present study, we succeeded in crystallizing tyrosinase with the help of the caddie protein ORF378. We determined the crystal structure of tyrosinase in a complex with ORF378 by the multiple isomorphous replacement method including the anomalous scattering effect. Furthermore, we obtained the met form of Cu(II)-bound tyrosinase complexed with ORF378 by soaking the native crystal in a $CuSO_4$ solution and that of its deoxy and oxy forms by soaking the met form crystal in a solution containing NH_2OH and H_2O_2, respectively. In the solution state, ORF378 is liberated from the complex by the addition of Cu(II); however, in the crystalline state, it is not. This might be due to the molecular packing effect in the crystal. In the present study, we show the structure of tyrosinase, which was determined as the first crystal structure among all tyrosinases from prokaryote and eukaryote.

MATERIALS AND METHODS

Crystallography of Copper-free Tyrosinase Complexed with ORF378—The expression and purification of the complex have been described previously (20). Before crystallization, the protein solution was dialyzed against a 20 mM Tris-HCl buffer (pH 7.9) containing 0.2 M NaCl and concentrated to 10 mg/ml using the Macrosep 3K (PALL). Crystals of tyrosinase in complex with ORF378 were obtained by the sitting drop vapor diffusion method using two different crystallization conditions. A precipitant solution containing 20% polyethylene glycol 4000, 0.1 M ammonium chloride, and 0.1 M Na-Hepes (pH 7.0) generated monoclinic $P2_1$ crystals with unit cell dimensions of $a = 58.9$ Å, $b = 93.2$ Å, $c = 65.6$ Å, and $\beta = 93.8°$, with two complexes/asymmetric unit. On the other hand, a precipitant solution containing 20% polyethylene glycol 3350, 0.2 M sodium nitrate, and 0.1 M Na-Hepes (pH 6.5) generated orthorhombic $P2_12_12$ crystals with unit cell dimensions of $a = 64.7$ Å, $b = 96.7$ Å, and $c = 54.6$ Å, with one complex/asymmetric unit. Because orthorhombic crystals diffracted to higher resolution than monoclinic ones and could be easily prepared by the microseeding method, later crystallographic analysis was mainly conducted using orthorhombic crystals.

All of the x-ray data were collected while the crystals were cooling under a nitrogen gas stream (100 K). Before flash cooling, crystals were soaked in a cryoprotectant solution containing a 5–15% higher concentration of polyethylene glycol 3350 or 4000 than the precipitant solution. Moderate resolution data of the native crystals (monoclinic and orthorhombic) and heavy atom derivatives (orthorhombic) were collected using a high speed Rigaku R-AXIS VII imaging plate detector with Cu$K\alpha$ radiation generated by Rigaku FR-E SuperBright. The diffraction intensities on the imaging plate were integrated and scaled by the program CrystalClear. Very high resolution data of the orthorhombic crystal up to 1.20 Å were collected using synchrotron radiation adjusted to a wavelength of 0.6199 Å from the station BL41XU at SPring-8, Japan. Because saturation of the diffraction intensity occurred in the lower resolution bin, a second data set of the same crystal was collected using an attenuated beam, and the two data sets were then merged. The diffraction intensities were integrated on the CCD camera (Mar research) using the program Mosflm, and the scaling was done using the program Scala equipped in the CCP4 program suite (25).

The phase problem was solved using the SHARP program (26). Heavy atom derivatives were prepared by soaking the crystal in a reservoir solution containing each heavy atom reagent. Two derivatives (mercury and gold) were used for the phasing. The initial phase set was obtained using the multiple isomorphous replacement method including the anomalous scattering effect, and subsequently the density was modified using the solvent-flattening and histogram-matching method. The resulting Fourier map enabled us to build an initial model using the program Xfit in the XtalView software package (27). The model was refined by a combination of the simulated annealing (28) and conventional restrained refinement methods (29) using the CNS program (30). A subset of 5% of the reflections was used to monitor the free *R* factor (R_{free}) (31). Each refinement cycle included refinement of the positional parameters and individual isotropic *B* factors, correction using the flat bulk solvent model, revision of the model using the omit map, and addition of solvent molecules. When the *R* factor fell below 20%, the native data were changed to the 1.20 Å resolution data. Further rebuilding, addition of solvent molecules, modeling of an alternative conformation, and refinement using the program SHELXL-97 (32) yielded the current model. The current model contains two protein subunits, 393 water molecules, and 4 nitrate ions. In the tyrosinase part, the N-terminal residue and the C-terminal region including the artificially added polyhistidine tag were invisible in the electron density map. Therefore, the current tyrosinase model consists of residues Thr^2–Leu^{274}. On the other hand, residues Ala^{40}–Ala^{59} and Gly^{71}–Pro^{122} in ORF378, which explain only 52% of the total residues (73% of the residues in the mature portion), can be confirmed by the electron density map. The high flexibility of the leader peptide domain (Met^1–Ala^{40}) is not surprising, because it is deleted after the secretion in the original cell but does not function in the *E. coli* system. Similarly, a large portion of the invisible C-terminal region contains the artificially added polyhistidine sequence. But the flexibility of residues Arg^{60}–Gly^{70} in ORF378 may be associated with the transportation of copper ions, as discussed later. No residues, except Phe^{103} and Asn^{188} of tyrosinase, are in the forbidden region of the Ramachandran plot (33). Three Pro residues (Pro^{169}, Pro^{237}, and Pro^{253}) in tyrosinase form *cis* peptide bonds to each previous residue.

The structure of the tyrosinase complexed with the ORF378 in the monoclinic crystal was determined by the molecular replacement method using the program Amore in the CCP4 program suite (25). The start model used was a complex determined in the orthorhombic cell. The initial coordinates of the two complexes were obtained by rotation and translation function analyses, and refinement was then performed using the program CNS (30). Each complex structure in the final model is almost the same as the previous structure refined in the orthorhombic cell. Most importantly, the undefined regions in the orthorhombic crystalline system remain uncertain in the monoclinic one. This indicates that the flexibility of the regions represents a molecular feature but is not derived from the molecular packing effect in the crystalline lattice. Details of the data collection, phasing, and refinement statistics are shown in Table 1.

Crystallography of the Met Form of Cu(II)-bound Tyrosinase Complexed with ORF378—To investigate the copper-binding site in the model and the structural change caused by Cu(II) incorporation, we soaked the crystal in the reservoir solution containing 1 mM $CuSO_4$ for the given times. Soaking in Cu(II) for more than 18 h successfully resulted in the complete incorporation of the ion to the active site. Two Cu(II) ions (Cu^A and Cu^B) were clearly defined in the active site of tyrosinase (Fig. 1, *B* and *C*); Cu^A binds to the Nϵ nitrogen atoms of His^{38}, His^{54}, and His^{63}, and Cu^B binds to those of His^{190}, His^{194}, and His^{216}. Interestingly, the distance between the two Cu(II) ions in the catalytic center gradually shortened as the soaking time increased. By Cu(II) soaking for ~60 h, the distance converged to a constant value of 3.3 Å. Until now, only two crystal structures are available for the met form of type 3 copper proteins: one is the subunit-II of *Limulus polyphemus* hemocyanin (Protein Data Bank code 1LL1), and the other is *Ipomoea batatas* catechol oxidase (Protein Data Bank code 1BT3) (11). In the first case, the electron density was assigned to the presence of two bridging water molecules, whereas the presence of only one water molecule was

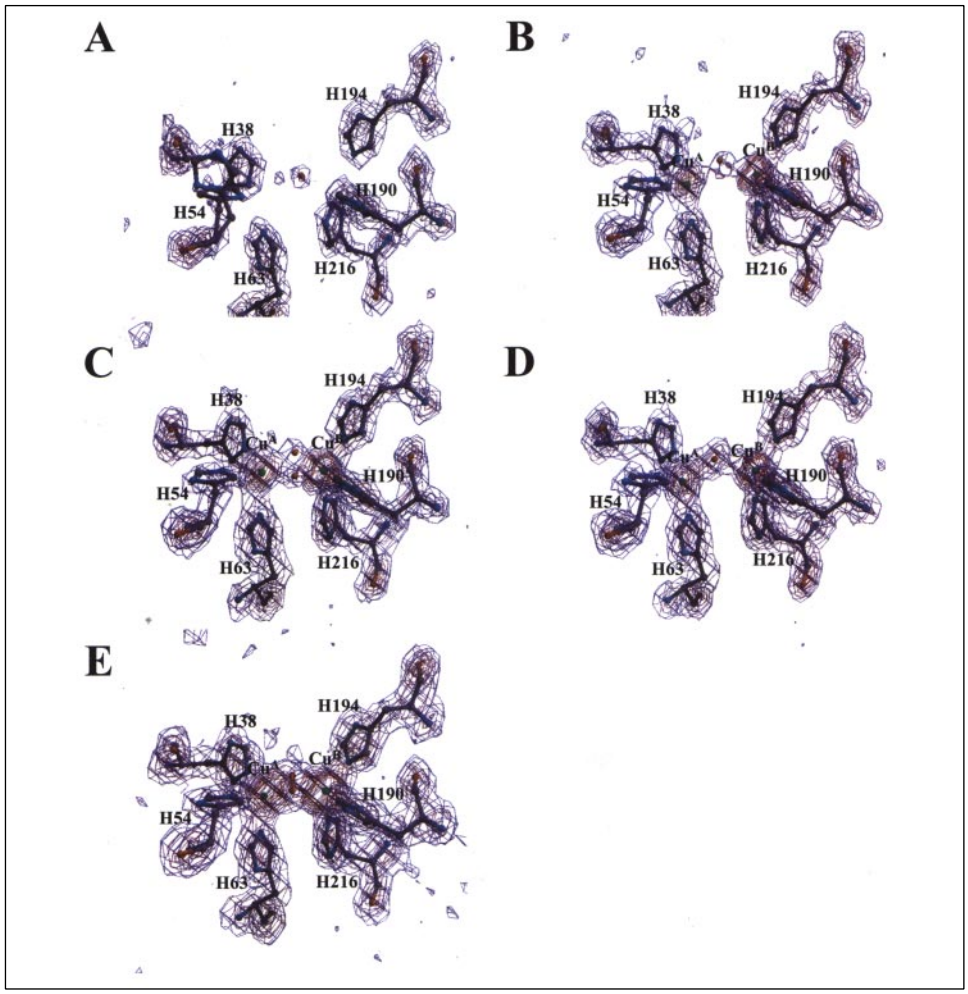

FIGURE 1. **Electron density around the dicopper center of tyrosinase.** *A*, electron density map around the dicopper center of copper-free tyrosinase complexed with ORF378. To emphasize the density, $F_o - F_c$ omit map was computed after removal of six His residues participating in copper binding and one water molecule. *B* and *C*, electron density map around the dicopper center of the met forms I (*B*) and II (*C*) of tyrosinase complexed with ORF378. The omit map was computed after removal of six His residues, two copper ions, and the bridging molecule. *D* and *E*, electron density map around the dicopper center of the deoxy (*D*) and oxy forms (*E*) of tyrosinase complexed with ORF378, prepared by the treatment with NH_2OH and H_2O_2, respectively. The omit map was computed after removal of six His residues, two copper ions, and the bridging molecule (water and peroxide ion).

assumed in the latter case. In our experiments, Cu(II)-soaking for less than 60 h gave a 1BT3-like met form, whereas soaking for a longer time gave a 1LL1-like met form. Hereafter, we name the former and the latter as met forms I and II, respectively. Moreover, two to three additional Cu(II) ions were identified, because the *B* factors were extremely low when they were assumed to be water. One of the additional ions, called the third Cu(II) ion in the text, binds to the Nϵ atom of His^{82} of ORF378 and is most frequently identified in the Cu(II)-bound structures obtained by soaking in Cu(II) solution for a short time (less than 80 h). With the increase of the soaking time, the third Cu(II)-binding site was partially occupied, and the fourth Cu(II)-binding site alternatively emerged. With further soaking, the Cu(II) ions were found only in the fourth Cu(II)-binding site. The fourth Cu(II) ion binds to the Nϵ atoms from His^{82} and His^{97} of ORF378 and the sulfur atom from Met^{84} of ORF378 similarly to the type 1 copper-binding protein. The fifth Cu(II) ion binds to the Nϵ atom of His^{180} of tyrosinase, and the sixth locates in the fully solvent region. The fifth and sixth Cu(II) ions are not constantly found among the Cu(II)-soaked structures. Details of the data collection and refinement statistics are shown in Table 1.

Crystallography of the Copper-bound Tyrosinase Complexed with ORF378 Prepared by Soaking in a Solution Containing the Redox Reagents—To determine the structure of deoxy form of tyrosinase, we anaerobically soaked the crystal in a reservoir solution containing 10 mM NH_2OH for 10 min, after soaking in 1 mM $CuSO_4$ for 69 h. Soaking in NH_2OH for about 5 min changed the crystal color from pale blue to pale yellow. Further soaking for more than 20 min generated cracks in the crystal, and the quality of the diffraction data became worse. On the other hand, the incorporation of a copper ion was not observed by soaking the crystal in a reservoir solution containing both 1 mM $CuSO_4$ and 10 mM NH_2OH for 40 h. This means that although the Cu(II) ion is introduced into the active site of tyrosinase, the Cu(I) ion is not. The distance between Cu^A and Cu^B at the active site in the deoxy form was clearly longer than that in the met form II. Because the electron density for a bridging solvent atom is rather strong, it is not likely to be a water molecule (Fig. 1*D*). However, we assumed that the atom was a water molecule because a more proper assignment was impossible.

On the other hand, we aerobically soaked the crystal in a reservoir solution containing 10 mM H_2O_2 for 20 min after soaking in 1 mM $CuSO_4$ for 76 h. After 5 min of soaking, the crystal color changed from pale blue to pale green. After additional soaking for more than 30 min, several cracks were observed in the crystal, and the quality of the diffraction data were worse. A bridging solvent atom might be a peroxide ion because the assignment gave clearer electron density than the assignment of two water molecules seen in the met form II (Fig. 1*E*). Therefore, the current structure is suggested to be the oxy form of tyrosinase in complex with ORF378. Details of the data collection and refinement statistics are shown in Table 1.

RESULTS AND DISCUSSION

Overview of the Structure—We determined the first crystal structure of tyrosinase, which is complexed with the caddie protein ORF378, at

TABLE 1
Data collection, phasing, and refinement statistics

	Native 1	Mercury	Gold	Native 2	Native 3	Met I	Met II	Deoxy	Oxy
Space group	$P2_12_12$	$P2_12_12$	$P2_12_12$	$P2_1$	$P2_12_12$	$P2_12_12$	$P2_12_12$	$P2_12_12$	$P2_12_12$
Data collection									
Soaking conditions									
Reagent		EMTS[a]	$KAu(CN)_2$			$CuSO_4$	$CuSO_4$	$CuSO_4/NH_2OH$	$CuSO_4/H_2O_2$
Concentration (mM)		10	10			1	1	1/10	1/10
Time		24 h	21 h			37 h	6 month	69 h/10 min	76 h/20 min
X-ray	R-AXIS VII	R-AXIS VII	R-AXIS VII	R-AXIS VII	BL41XU	BL41XU	R-AXIS VII	R-AXIS VII	R-AXIS VII
Wavelength (Å)	1.54184	1.54184	1.54184	1.54184	0.6199	0.9000	1.54184	1.54184	1.54184
Resolution (Å)	1.50	1.80	2.20	2.02	1.20	1.33	1.71	1.60	1.80
Unique reflection	55,522	32,646	18,130	46,161	104,674	78,955	37,596	47,376	32,279
Redundancy[b]	3.34 (3.10)	3.42 (3.24)	3.40 (3.36)	5.01 (4.34)	8.10 (5.10)	7.58 (3.89)	3.26 (3.30)	3.43 (3.28)	3.20 (3.08)
Completeness (%)[b]	99.1 (97.2)	99.5 (98.9)	99.6 (99.8)	99.6 (98.9)	97.8 (99.0)	97.3 (93.2)	97.7 (98.4)	99.6 (98.1)	98.5 (98.8)
R_{merge} (%)[b,c]	4.1 (30.4)	5.0 (19.6)	9.6 (27.4)	12.5 (27.8)	8.0 (36.6)	7.4 (32.8)	3.7 (30.8)	6.7 (30.7)	5.0 (28.0)
I/σ[a]	10.8 (2.2)	13.5 (5.0)	7.1 (2.8)	7.3 (3.4)	5.9 (2.0)	6.4 (2.4)	15.3 (3.7)	11.6 (2.9)	10.7 (3.1)
Phasing									
Heavy atom sites		2	3						
Phasing power									
Isomorphous		0.651	0.749						
Anomalous		0.250	0.225						
Refinement									
Resolution (Å)				30–2.02	30–1.20	30–1.33	30–1.71	30–1.60	30–1.80
Used reflections				45,956	100,937	75,060	36,981	44,216	32,193
Total atoms				6,033	3,220	3,128	3,081	3,146	3,016
R (%)				20.1	18.0	19.1	19.4	21.5	21.0
R_{free} (%)				29.1	20.8	21.8	24.1	26.3	24.9
Root mean square deviations from ideal[d]									
Bond length (Å)				0.006	0.013	0.006	0.007	0.009	0.009
Bond angle (°)				1.2	2.3	1.3	1.2	1.3	1.3

[a] EMTS, ethylmercuricthiosalicylic acid.
[b] The values in parentheses are for the highest resolution bin.
[c] $R_{merge} = \Sigma|I - <I>|/\Sigma I$, where I is the observed intensity, and $<I>$ is the mean value of I.
[d] The ideal values are defined by Engh and Huber (47).

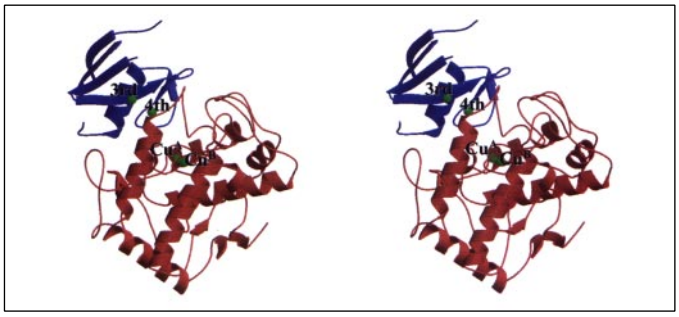

FIGURE 2. **Overall structure of tyrosinase complexed with ORF378.** Stereo representation of the ribbon view of the copper-bound form of the *S. castaneoglobisporus* tyrosinase complexed with ORF378. Tyrosinase and ORF378 are shown in *red* and *blue*, respectively. Four of the six identified copper ions are indicated by *green spheres*. Two of them are located at the dicopper center of tyrosinase, and the third copper ion is bound at the molecular surface of ORF378. The fourth copper ion exists in the interior of ORF378.

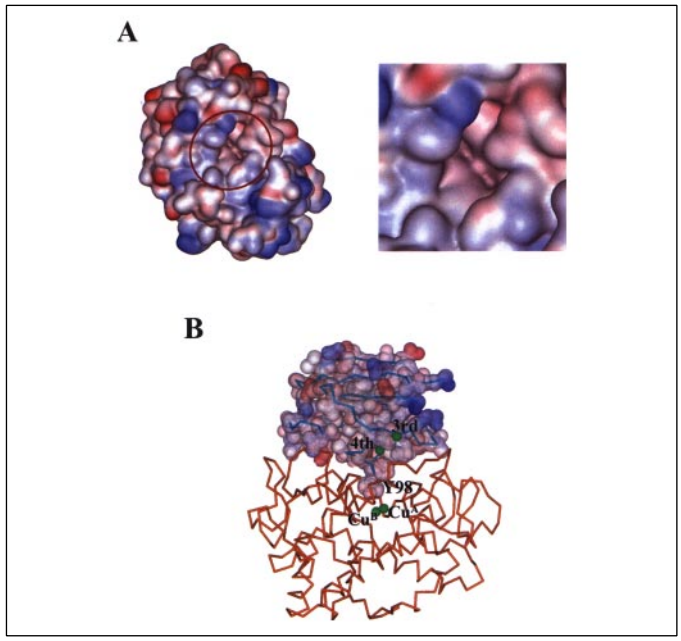

FIGURE 3. **Molecular surfaces of tyrosinase (*A*) and ORF378 (*B*).** *A*, area surrounded by a circle is revealed under magnification. The area contains the substrate-binding pocket of tyrosinase. *Red* and *blue* show the negative and positive electrostatic potential, respectively. *B*, *orange*, *cyan*, and *green* represent tyrosinase, ORF378, and copper ions, respectively. Tyr^{98} of ORF378 is present in the substrate-binding pocket of tyrosinase.

1.2–1.8 Å resolution (Table 1). Tyrosinase, complexed with ORF378, is ellipsoid in shape and has dimensions of 40 × 55 × 60 Å (Fig. 2).

Tyrosinase takes α-helical structures with the core of the enzyme, which is formed by a four-helix bundle (α2, α3, α6, and α7 helices). The catalytic dinuclear copper center is lodged in the helical bundle (Fig. 2). Each of the two copper ions in an active site is coordinated by three His residues (Fig. 1, *B–E*), which are derived from the four helices of the α-bundle except His^{54}. One copper ion (designated Cu^A) is coordinated by His^{38}, His^{54}, and His^{63}. His^{38} and His^{63} are located in the middle of α2 and α3, respectively. The second copper ion (Cu^B) is coordinated by His^{190}, His^{194}, and His^{216}. The residues His^{190} and His^{194} are at the beginning and in the middle of α6, respectively, and His^{216} is in the middle of α7. This dicopper center is located at the bottom of the large concavity as a putative substrate-binding pocket (Fig. 3*A*), which is formed by the hydrophobic residues. In addition to the helical structure, tyrosinase has a few β-structures, as judged from the backbone torsion angles. In these, only the N- and C-terminal β-strands form a sheet structure.

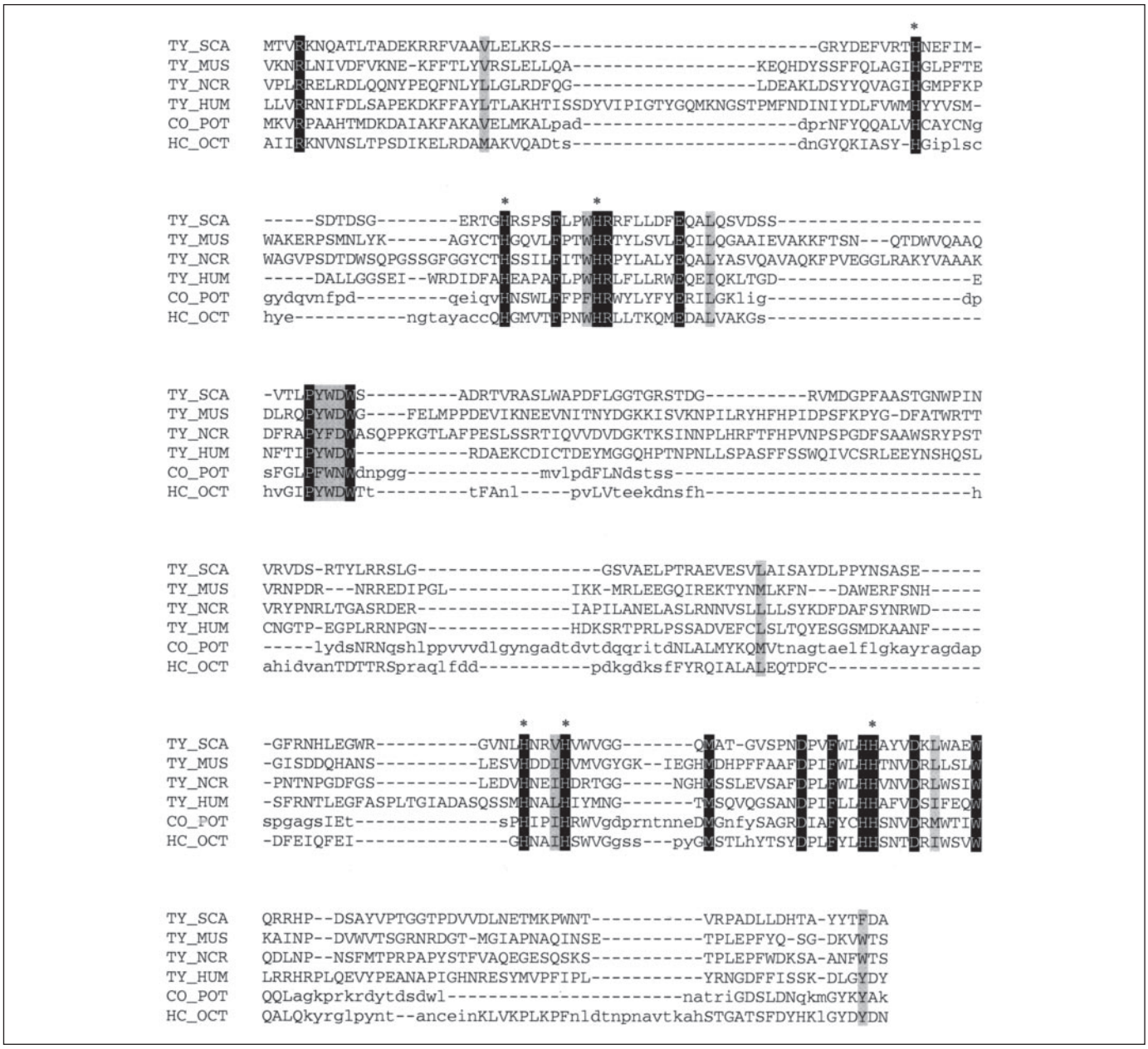

FIGURE 4. **Multiple sequence alignment of the type 3 copper proteins.** *TY_SCA* indicates the amino acid sequence of the *S. castaneoglobisporus* tyrosinase. The other sequences are taken from the GenBank™ data base: *TY_HUM*, human tyrosinase; *TY_MUS*, *A. bisporus* (mushroom) tyrosinase; *TY_NCR*, *N. crassa* tyrosinase; *CO_POT*, potato catechol oxidase; *HC_OCT*, octopus hemocyanin. Structurally superimposable residues in *CO_POT* and *HC_OCT* are shown by *capital letters*. The identical and conserved residues are displayed in *black* and *gray shading*, respectively. The *asterisks* indicate the His residues participating in copper binding.

Although the amino acid sequence of tyrosinase respectively has only 25.3 and 26.0% identities with those of the *I. batatas* catechol oxidase (11) and the odg domain of the *Octopus dofleini* hemocyanin (10), which have a type 3 copper center (Fig. 4), its overall structure is quite similar to theirs (Fig. 5*A*). The root mean square value of the positional differences of the main chain atoms in tyrosinase and the *Ipomoea* catechol oxidase is 0.94 Å for 138 matched residues, and that in tyrosinase and the *Octopus* hemocyanin is 1.34 Å for 172 residues. Among these three proteins, a high degree of conservation is observed in the core domain composed of the α-bundle. The tyrosinase and hemocyanins from *Panulirus interruputus* (5, 6) and *L. polyphemus* (7–9) show no significant homology and no resemblance in their structures, but the catalytic core domains of these proteins are superimposable.

ORF378, a caddie protein that covers the molecular surface of tyrosinase, seems to prevent substrate binding to the active site of tyrosinase (Fig. 3*B*). This could imply that the folding of the catalytic center of tyrosinase occurs at an earlier step than that for the other parts of the enzyme in the process of maturation. ORF378 has one six-stranded β-sheet, largely twisted at strand β4, and one α-helix, which is surrounded by a twisted sheet. ORF378 has no sequence similarity with proteins structurally determined. According to the results obtained using the DALI program (34), however, ORF378 has a significant structural similarity with the SH2 domain (Fig. 5*B*), which is contained in the proteins with respect to the signal transduction, such as a growth factor-bound protein (35), tyrosine kinase (36, 37), tyrosine phosphatase (38), a T-cell signal transduction molecule (39), and phospholipase C (40).

However, the typical SH2 domain has five-stranded β-sheets and two α-helices flanking the sheet. Because the N-terminal α-helix in the SH2 domain is replaced by a β1-strand in ORF378, the latter protein consists of a six-stranded β-sheet. Judging from the similarity between ORF378 and the SH2 domain, these proteins might have evolved from the same ancestor. ORF378 and the SH2 domain have a key process in common with tyrosine: ORF378 assists in the folding of tyrosinase, which is necessary to metabolize tyrosine toward melanin synthesis, and some SH2 domain-harboring proteins catalyze the phosphorylation or dephosphorylation of the tyrosine residue.

Interaction between Tyrosinase and ORF378—The decreased molecular surface area on the complex formation between tyrosinase and ORF378 is calculated to be 980 Å^2, which is apparently lower than that caused by the normal dimer formation, suggesting that the interaction between both the proteins is considerably weak. This conclusion is reached on the basis of the observation that several residues in the interaction surface of the copper-free tyrosinase/ORF378 complex, such as Ile^{42}, His^{54}, and Arg^{140} of tyrosinase and Val^{94} of ORF378, take disordered conformations. In addition, amino acid residues, defined in the electron density, are only 52% of the total residues in ORF378. The averaged *B* factor of visible residues in ORF378 is higher than that of tyrosinase, indicating that ORF378 takes a flexible conformation. These results suggest that the current structure is an intermediate state before the activation of tyrosinase. Weak intermolecular interactions, observed in the structure of tyrosinase in a complex with the caddie protein, are also shown in the protease-propeptide complex (41, 42).

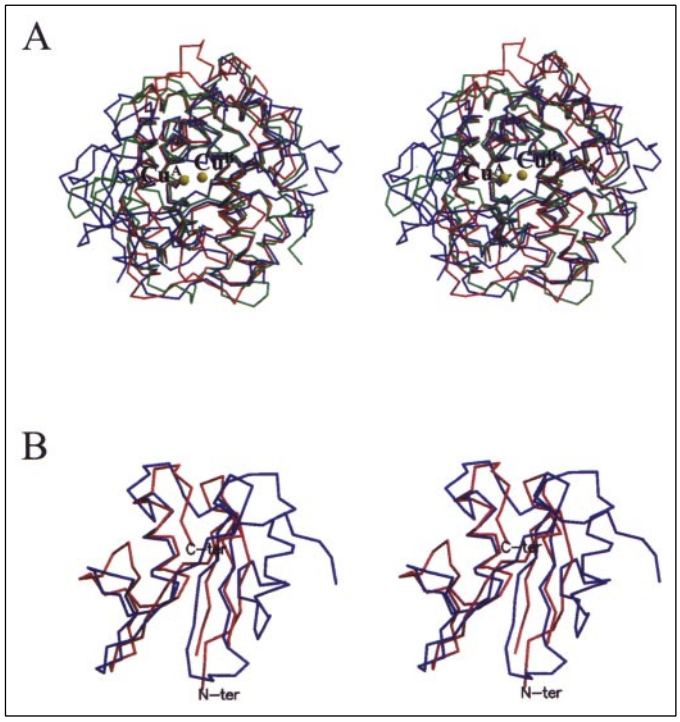

FIGURE 5. **Structural similarity.** *A*, stereo representation of the superposition of tyrosinase and structurally homologous proteins, potato catechol oxidase (Protein Data Bank code 1BT1) and octopus hemocyanin (Protein Data Bank code 1JS8). *Red*, *blue*, and *green* indicate the backbone traces of tyrosinase, catechol oxidase, and hemocyanin, respectively. The *yellow sphere* indicates the two copper ions in the catalytic center. To emphasize similarity, the C-terminal domain of hemocyanin is omitted from the figure. *B*, stereo view of the superposition of ORF378 and the SH2 domain in the growth factor-bound protein 2 (Protein Data Bank code 1GRI). *Red* and *blue* indicate the backbone trace of ORF378 and the SH2 domain in the growth factor-bound protein 2, respectively.

The interaction between tyrosinase and ORF378, which is mediated by Tyr^{98} from ORF378, is quite attractive. The amino acid protrudes away from the core region of ORF378 (Fig. 3*B*). The side chain of Tyr^{98} is accommodated in the substrate-binding pocket of tyrosinase. The phenol ring is stacked with the imidazole ring of His^{194} of tyrosinase, which is one of the Cu^B ligands (Fig. 6*A*). In addition, its phenolic hydroxyl forms a hydrogen bond with solvent atoms (water molecule or peroxide ion), which form a bridge with Cu^A and Cu^B in the active center of tyrosinase (Fig. 7, *B–E*). Furthermore, when compared with the catechol oxidase in a complex with a potent inhibitor, phenylthiourea, the Tyr^{98} ring is aligned perfectly with the aromatic ring of the inhibitor (Fig. 6, *A* and *B*). These results suggest that Tyr^{98} of ORF378 functions as a competitive inhibitor to the substrate tyrosine. But judging from an observation that tyrosine residue is not converted to *ortho*-diphenolic compound, Tyr^{98} may not take an intermediate conformation in the catalytic process. Because the size of substrate-binding pocket of tyrosinase is actually large (Fig. 3*A*), the substrate tyrosine may be accommodated into the pocket at various binding modes. Therefore, we cannot propose the reliable binding mode of the substrate. As proposed previously using molecular simulation (43, 44), the binding of phenolic oxygen to Cu^B may be necessary as the first process for the tyrosinase reaction.

Structural Change of the Tyrosinase Active Site—We analyzed the structural change on five forms of tyrosinase complexed with ORF378; one is a copper-free form, and the others are two met forms (I and II) and the oxy and deoxy forms of the copper-bound complex (Figs. 1 and 7). Cu(II) ions are observed to release ORF378 from the complex in solution but not in crystal. This may be due to the molecular packing effect in the crystal, which prevents the dissociation of ORF378. However, a slight rotational movement of ORF378 is observed by the addition of Cu(II) ions in the crystalline state. This movement is likely to exhibit the dissociation process of ORF378 from the complex. Structural changes at the active center of tyrosinase are also observed (Fig. 7). In the copper-free tyrosinase, the side chain of His^{54}, as one of the Cu^A ligands, is flexible, as proved by the presence of the disordered structure (Fig. 1*A*). The flexibility of His^{54} may be caused by the absence of a thioether bond, as found in catechol oxidase (Fig. 6*B*) and hemocyanin (Fig. 6*C*). On the other hand, the side chain is more rigid in the copper-

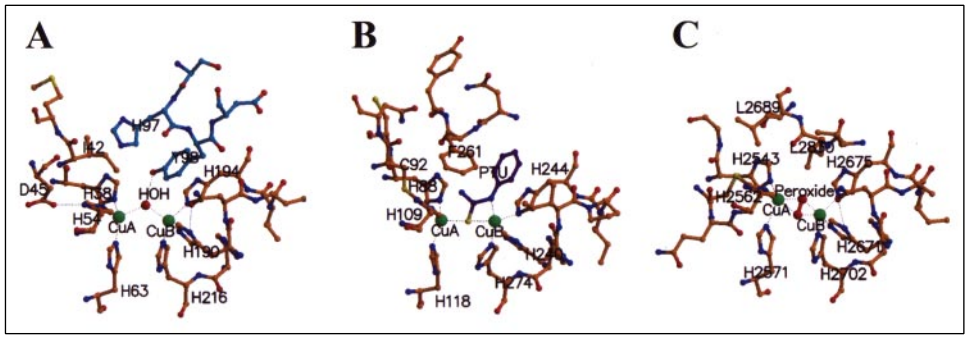

FIGURE 6. **The active centers of tyrosinase and of structurally homologous proteins.** *A*, active center of the met form I of tyrosinase complexed with ORF378. Carbon atoms from the residues of tyrosinase and ORF378 are shown in *orange* and *cyan*, respectively. *B*, active center of the inhibitor-bound potato catechol oxidase. Carbon atoms from catechol oxidase and inhibitor (phenylthiourea, *PTU*) are shown in *orange* and *purple*, respectively. *C*, active center of the oxy form of the octopus hemocyanin. Carbon atoms from hemocyanin are shown in *orange*.

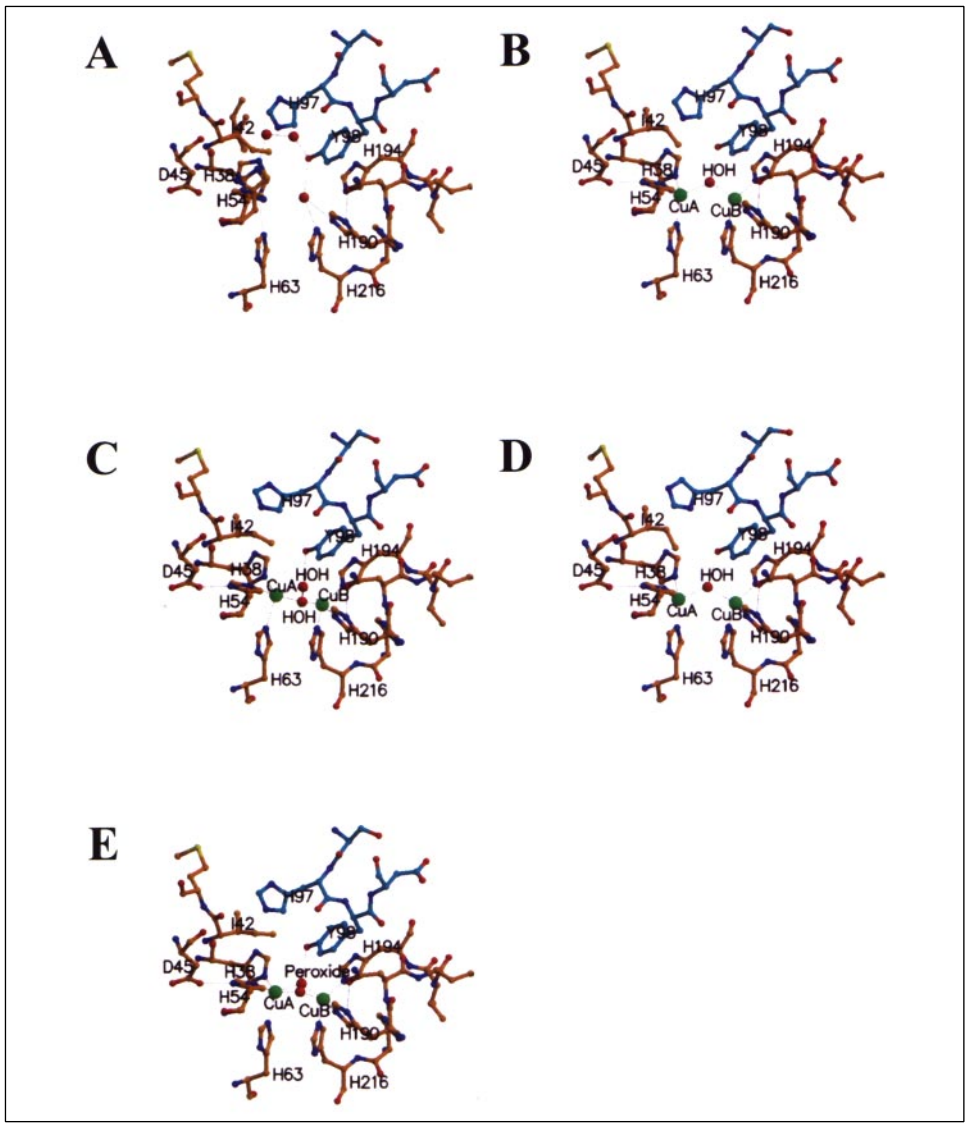

FIGURE 7. **Conformational changes of the active center of tyrosinase caused by copper and dioxygen binding.** *A–C* indicate the active centers of the copper-free form, met form I, and met form II of tyrosinase complexed with ORF378, respectively. *D* and *E* indicate the active center of the deoxy and oxy forms of tyrosinase complexed with ORF378, respectively. The carbon atoms from the residues of tyrosinase and ORF378 are shown in *orange* and *cyan*, respectively.

bound tyrosinase (Fig. 1, *B–E*). However, even in the copper-bound structures, the His^{54} atoms have higher *B* factors than those of the other five copper ligand residues. Because of the high mobility of His^{54}, Cu^A is less stable than Cu^B.

By soaking the tyrosinase complexed with ORF378 in a $CuSO_4$ solution for over 18 h, the met form was obtained (Fig. 1, *B* and *C*). We observed that the distance between the two Cu(II) ions present in the met form was gradually shortened to 3.3 Å by increasing the soaking time. However, when the soaking time was less than 60 h, the time at which the met form I is formed, the corresponding distance is ~3.9 Å. As a result, the Cu(II) ions were observed to form a bridge with one water molecule. On the other hand, under the soaking condition, which gives the met form II where the distance was converged to 3.3 Å, the copper ions formed bridges with two water molecules. For tuning up the catalytic reaction of tyrosinase, it may be necessary for the distance between Cu^A and Cu^B in the catalytic center to be flexible. The conversion of the met form I to the met form II induced a more stable conformation at the catalytic center. In this study, we examined the flexibility of His^{54} and Cu^A and Cu^B, with respect to the mean *B* factors for all protein atoms. As a result, we found that the flexibility of Cu^B is almost constant, whereas that of Cu^A and His^{54} is largely varied. In the met form II, Cu^A and His^{54} have structural stability, like Cu^B.

In the met form I (Fig. 7*B*), six His ligands and a bridging solvent complete the four-coordinated trigonal coordination for both Cu(II) atoms with His^{54} and His^{190} in the apical position of the coordination polyhedron for Cu^A and Cu^B, respectively. On the other hand, in the met form II (Fig. 7*C*), Cu^A is in the distorted tetragonal-pyramidal coordination with His^{38}, His^{63}, and two waters in the equatorial position and His^{54} in an axial position. Because a sixth coordination site is located in the interior of the enzyme, it is not bound to a solvent atom. Cu^B is also in distorted tetragonal-pyramidal coordination with His^{194}, His^{216}, and two waters in the equatorial position and His^{190} in an axial position, but the vacant sixth coordination site is located in the substrate-binding pocket.

We formed the deoxy form of the Cu(I)-bound tyrosinase by the addition of NH_2OH under anaerobiosis after Cu(II)-soaking for 69 h (Fig. 1*D*). After soaking for 69 h, the time at which the met form II is formed, the distance between two Cu(II) ions is at a minimum. However, the distance in the deoxy form increased to 4.1 Å. The space expanded between the copper ions may be useful to accommodate dioxygen in the catalytic center. A bridging solvent is equidistant (2.3 Å) from Cu^A and Cu^B, and the coordination geometry for the copper ions in the deoxy form is similar to that in the met form I (Fig. 7*D*). This is different from what was observed in the active center of the deoxy form

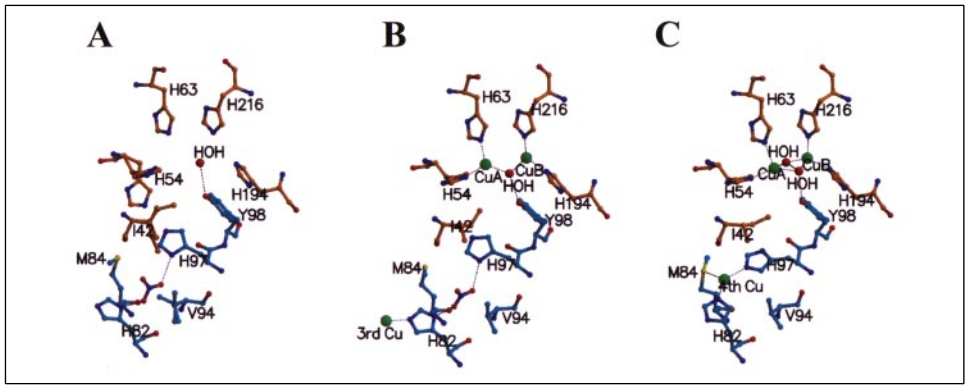

FIGURE 8. **Third and fourth copper-binding sites and clustered His residues.** *A* shows the partial atomic models of the copper-free tyrosinase complexed with ORF378. Ile^{42} and His^{54} of tyrosinase and Val^{94} of ORF378 have disordered structures. The molecule bridging between His^{82} and His^{97} of ORF378 is a nitrate ion. *B* and *C* show the partial atomic models of the met form of tyrosinase complexed with ORF378 prepared by soaking in a $CuSO_4$ solution for 37 h and 6 months, respectively. In *B*, the third Cu(II) binds to the Nϵ atom of His^{82} of ORF378. In *C*, although the third Cu(II)-binding site was hardly occupied, the fourth Cu(II) ion, which binds to the Nϵ atoms from His^{82} and His^{97} of ORF378 and the sulfur atom from Met^{84} of ORF378, was observed. Carbon atoms from the residues of tyrosinase and ORF378 are shown in *orange* and *cyan*, respectively.

of catechol oxidase (11); that is, the distance between the bridging solvent and Cu^A is shorter than that between the solvent and Cu^B. Furthermore, the catalytic center in the deoxy form is structurally stable, like that of the met form II. We point out that although the distance between Cu^A and Cu^B of the catalytic center in the met form I is approximately the same as that in the deoxy form, the stability of the catalytic center of the former is obviously lower than that of the latter.

In contrast, the oxy form of the Cu(II)-bound tyrosinase was formed by the addition of hydrogen peroxide (H_2O_2) after Cu(II)-soaking for 76 h (Fig. 1*E*). Although it is difficult to distinguish the oxy form from the met form II by the electron density, the distance between the two bridging solvent atoms of the former form is somewhat shorter than that of the latter. Therefore, we assumed that the density for the bridging solvent is a peroxide ion. In fact, the oxy form of tyrosinase formed by the addition of H_2O_2 was confirmed by its typical UV-visible spectrum at 350 nm in solution. In the oxy form structure, the peroxide ion binds in a bridging side-on μ-η^2:η^2 binding mode (Fig. 7*E*). The distance between the Cu(II) ions in the oxy form is 3.4 Å, and the coordination geometry is almost identical to that in the met form II. However, the dicopper center of the oxy form is more unstable than that of the met form II. The difference electron density around the His^{54} side chain indicates that the residue is disordered, as seen in the copper-free form. This observation may correlate with the high reactivity of the oxy form of tyrosinase.

Structural Evidence That ORF378 Functions as a Cu(II) Transporter for Tyrosinase—We have suggested that ORF378 serves as a transporter of Cu(II) ions to the catalytic site of apotyrosinase (copper-free tyrosinase). This study presents structural evidence that ORF378 plays a role in the transport of two Cu(II) ions to apotyrosinase, as demonstrated by the x-ray diffraction analysis of about 30 crystals of copper-bound tyrosinase complexed with ORF378 prepared under different soaking conditions. The structural analysis of these crystals demonstrated that the complex has Cu(II)-binding sites in addition to a catalytic center in which two Cu(II) ions are accommodated.

The third Cu(II) ion, which is most frequently identified in the crystals soaked in a Cu(II) solution for less than 80 h, binds to the Nϵ atom from His^{82} of ORF378. This site is on the molecular surface of ORF378 (Fig. 8*B*), and the Nδ atom of the His^{82} side chain forms a hydrogen bond with the Nδ atom of His^{97} of ORF378 by the mediation of the nitrate ion, which is derived from a precipitant solution. However, by soaking crystals in a $CuSO_4$ solution for a longer time, the third binding site for the Cu(II) ion was partially occupied, and the fourth Cu(II) ion, which binds to the Nϵ atoms from His^{82} and His^{97} of ORF378, alternatively emerged (Fig. 8*C*). The fourth Cu(II) ion was also found to bind to the sulfur atom from Met^{84} of ORF378 in a manner similar to that of the type 1 copper-binding protein. To make the fourth Cu(II)-binding site, the imidazole rings of His^{82} and His^{97} must be rotated around the bond between their Cβ and Cγ atoms. By soaking crystals in a $CuSO_4$ solution for 6 months, the fourth binding site for the Cu(II) ion was completely occupied, and the third binding site was emptied. Thus, we could observe the movement of the additional Cu(II) ion in a time-dependent manner.

The imidazole ring of His^{97} of ORF378 is located near the side chain of His^{54} of tyrosinase. Especially in the copper-free tyrosinase complexed with ORF378, the alternative His^{54} side chain of tyrosinase is closer to the His^{97} side chain of ORF378 (Fig. 8*A*). The clustered His residues, which extend from the molecular surface of ORF378 to the active center of tyrosinase, may bind to Cu(II) atoms in the process of transferring the metal ions to the catalytic center.

It has been reported that, when His^{102} and His^{117} of *S. antibioticus* ORF438, which correspond to His^{82} and His^{97} of *S. castaneoglobisporus* ORF378, were replaced by Leu and Asp, respectively, the copper transferring activity of ORF438 was reduced (19). A copper ion, which is illustrated as the third position in Fig. 3*B*, may first bind for transportation of copper ions to tyrosinase to His^{82} located on the surface of ORF378. In general, an atmosphere for metal binding should take negative charge, whereas electrostatic potential around the third position for Cu(II)-binding is neutral. This suggests that the third position is not actually located on the surface of ORF378. ORF378 contains four His residues (His^{64}, His^{65}, His^{66}, and His^{68}), but the residues are invisible in the electron density map. Because the disordered residues are likely to be positioned near the third copper-binding site, they might function as the initial copper-binding site.

Comparison with Proteins Having a Type 3 Copper Center—Tyrosinase belongs to the protein family having a type 3 copper center, as do catechol oxidase (11) and hemocyanin (5–10). The reasons for the different functions exhibited by these proteins pose an interesting query. For example, hemocyanin plays a significant role in the transportation of oxygen into arthropods and mollusks. The protein has a domain that shields the access to the dicopper center of the protein (Fig. 6*C*). Because the domain interferes with the binding of the substrate, hemocyanin can play only one role, namely, that of an oxygen transporter. The dicopper center of both catechol oxidase and tyrosinase is near the molecular surface, a useful location to ensure that a substrate can access each catalytic site (Fig. 6, *A* and *B*).

Both tyrosinase and catechol oxidase catalyze the oxidation of *ortho*-diphenols to the corresponding quinones, but the latter enzyme lacks the monooxygenase activity to convert monophenols to *ortho*-diphenols. The structure and function of tyrosinase have been compared with those of catechol oxidase. One of the most attractive differences may be the vacant space of the substrate-binding pocket. The Phe^{261} side chain in the active site of catechol oxidase, which is located just above the Cu^A site, seems to partially prevent substrate binding (Fig. 6*B*). In contrast,

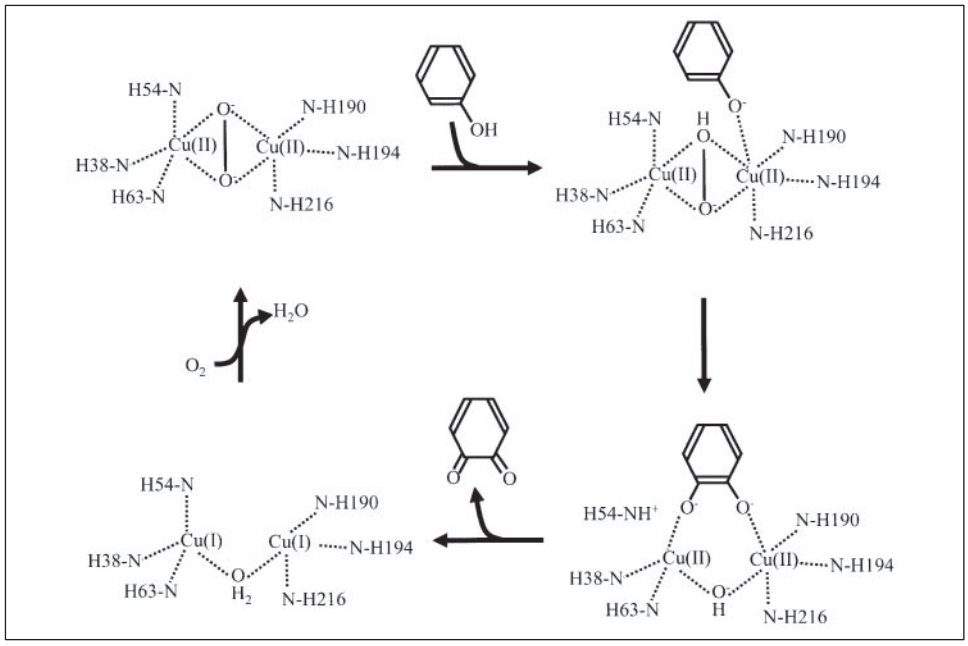

FIGURE 9. **Structure-based catalytic mechanism of tyrosinase.** The oxy form of tyrosinase catalyzes the conversion of monophenol to the corresponding quinone through the *ortho*-diphenol formation. In this scheme, His^{54} is released from the Cu^A site, resulting in the formation of the bidentate intermediate. The met and oxy forms of tyrosinase can catalyze the conversion of *ortho*-diphenol to the corresponding quinone. This reaction should progress similarly to that of catechol oxidase.

the substrate-binding pocket of tyrosinase has a larger vacant space above the dicopper center, if ORF378 complexed with tyrosinase is liberated from tyrosinase (Fig. 6*A*).

His^{54} of tyrosinase, which is one of the Cu^A ligands, differs obviously from the corresponding His^{109} of catechol oxidase from sweet potato. In copper-free tyrosinase, complexed with ORF378, the His^{54} residue takes two conformations: one is exactly the same as the conformation observed in the copper-bound form, but the other, a side chain of His^{54}, protrudes toward the molecular surface (Fig. 7*A*). In catechol oxidase (11), His^{109} is fixed by the unusual covalent bond formed between the Cϵ atom of His^{109} and the sulfur atom of Cys^{92} (Fig. 6*B*). The catalytic specificity of tyrosinase or cathecol oxidase may depend on the flexibility of His^{54} or the inflexibility of His^{109}, respectively.

The thioether bond is also found in the structure of hemocyanin. In the *Octopus* hemocyanin (10), the thioether bond is formed with a Cϵ atom of His^{2562}, which is the counterpart of His^{109} of catechol oxidase (Fig. 6*C*). However, the sulfur atom is provided from a structurally different Cys residue. As judged from the sequence similarity to the *Octopus* hemocyanin, tyrosinases from *Neurospora crassa* (45) and *Agaricus bisporus* (46) might have the thioether bond in the active site (Fig. 4). The hypothesis will be confirmed by the determination of their crystal structures.

Implication for the Catalytic Mechanism—Tyrosinase can catalyze the *ortho*-hydroxylation of monophenol and the conversion of the *ortho*-diphenols to the corresponding quinones. Based on the crystal structure of tyrosinase obtained in the present study, we can describe the tyrosinase-specific catalytic mechanism in detail (Fig. 9). At first, a peroxide ion, which forms a bridge with two Cu(II) ions in the oxy form of tyrosinase, acts as a catalytic base. As a result, a proton is abstracted from the phenolic hydroxyl. Subsequently, the deprotonated oxygen atom of monophenol binds to Cu^B at the sixth coordination site. At this time, Cu^B is hexa-coordinated by a tetragonal bipyramidal cage, and an *ortho*-carbon of the substrate approaches the peroxide ion. One of two peroxide oxygens is then added to the *ortho*-carbon of monophenol. This monooxygenase reaction would be accelerated by the formation of a stable intermediate, in which newly generated oxygen atoms of diphenol bind to Cu^A. To form this state, His^{54}, which is an axial ligand to Cu^A, must be released from the current position. This assumption is derived from the flexible feature of the residue His^{54} in the copper-free and Cu(II)-bound oxy forms. Simultaneously, His^{54} can act as a catalytic base for the deprotonation from the substrate. The resulting intermediate has the advantage of easy translation of electrons, resulting in the formation of the deoxy form of tyrosinase and quinone.

Our proposed scheme does not fit the case of catechol oxidase (11) because the bidentate intermediate cannot be formed because of the fixed conformation of His^{109}, which corresponds to His^{54} of tyrosinase, and the presence of the Phe^{261} lying just above the Cu^A site, which is vacant in the tyrosinase structure (Fig. 6, *A* and *B*). There is a consensus (1, 44) that the oxy form of tyrosinase can catalyze both the monooxygenase and oxidase reactions, whereas the met form lacks the monooxygenase activity. This can be explained as follows: the bidentate intermediate formation, which is permitted only by the oxy form, is essential for the monooxygenase reaction, but the mono-dentate intermediate, which is formed by the met form, is sufficient for an oxidase reaction, as proposed for catechol oxidase. Therefore, some compounds that bind to two Cu(II) ions in the bidentate form might be potent inhibitors of tyrosinase.

Acknowledgments—We are grateful to Drs. J. Hoseki, M. Kanagawa, and N. Nakagawa (technicians with the Metabolism Group, Protein 3000 Project, Japan) for valuable help with the x-ray data collection. We also thank Drs. H. Sakai and M. Kawamoto (beam-line assistants of BL41XU, SPring-8, Japan) for kind help with x-ray data collection.

REFERENCES

1. Solomon, E. I., Sundaram, U. M., and Machonkin, T. E. (1996) *Chem. Rev.* **96,** 2563–2606
2. Oetting, W. S. (2000) *Pigment Cell Res.* **13,** 320–325
3. Xu, Y., Stokes, A. H., Roskoski, R. J., and Vrana, K. E. (1998) *J. Neurosci. Res.* **54,** 691–697
4. Asanuma, M., Miyazaki, I., and Ogawa, N. (2003) *Neurotox. Res.* **5,** 165–176
5. Volbeda, A., Feiters, M. C., Vincent, M. G., Bouwman, E., Dobson, B., Kalk, K. H., Reedijk, J., and Hol, W. G. (1989) *Eur. J. Biochem.* **181,** 669–673
6. Volbeda, A., and Hol, W. G. (1989) *J. Mol. Biol.* **209,** 249–279
7. Hazes, B., Magnus, K. A., Bonaventura, C., Bonaventura, J., Dauter, Z., Kalk, K. H., and Hol, W. G. (1993) *Protein Sci.* **2,** 597–619
8. Hazes, B., Magnus, K. A., Kalk, K. H., Bonaventura, C., and Hol, W. G. (1996) *J. Mol. Biol.* **262,** 532–541

9. Magnus, K. A., Hazes, B., Ton-That, H., Bonaventura, C., Bonaventura, J., and Hol, W. G. (1994) *Proteins* **19,** 302–309
10. Cuff, M. E., Miller, K. I., van Holde, K. E., and Hendrickson, W. A. (1998) *J. Mol. Biol.* **278,** 855–870
11. Klabunde, T., Eicken, C., Sacchettini, J. C., and Krebs, B. (1998) *Nat. Struct. Biol.* **5,** 1084–1090
12. Ikeda, K., Masujima, T., Suzuki, K., and Sugiyama, M. (1996) *Appl. Microbiol. Biotechnol.* **45,** 80–85
13. Ikeda, K., Masujima, T., and Sugiyama, M. (1996) *J. Biochem.* (*Tokyo*) **120,** 1141–1145
14. Katz, E., Thompson, C. J., and Hopwood, D. A. (1983) *J. Gen. Microbiol.* **129,** 2703–2714
15. Berman, V., Filpula, D., Herber, W., Bibb, M., and Katz, E. (1985) *Gene* (*Amst.*) **37,** 101–110
16. Huber, M., Hintermann, G., and Lerch, K. (1985) *Biochemistry* **24,** 6038–6044
17. Hintermann, G., Zatchej, M., and Hütter, R. (1985) *Mol. Gen. Genet.* **200,** 422–432
18. Chen, L. Y., Leu, W. M., Wang, K. T., and Lee, Y. H. W. (1992) *J. Biol. Chem.* **267,** 20100–20107
19. Chen, L. Y., Chen, M. Y., Leu, W. M., Tsai, T. Y., and Lee, Y. H. W. (1993) *J. Biol. Chem.* **268,** 18710–18716
20. Kohashi, P. Y., Kumagai, T., Matoba, Y., Yamamoto, A., Maruyama, M., and Sugiyama, M. (2004) *Protein Expression Purif.* **34,** 202–207
21. Harrenga, A., and Michel, H. (1999) *J. Biol. Chem.* **274,** 33296–33299
22. Hunte, C., Koepke, J., Lange, C., Rossmanith, T., and Michel, H. (2000) *Structure Fold. Des.* **8,** 669–684
23. Zhou, Y., Morais-Cabral, J. H., Kaufman, A., and MacKinnon, R. (2001) *Nature* **414,** 43–48
24. Dutzler, R., Campbell, E. B., and MacKinnon, R. (2003) *Science* **300,** 108–112
25. Collaborative Computational Project Number 4 (1994) *Acta Crystallogr. Sect. D Biol. Crystallogr.* **50,** 760–763
26. de la Fottelle, E., and Bricogne, G. (1997) *Methods Enzymol.* **276,** 472–494
27. McRee, D. E. (1992) *J. Mol. Graphics* **10,** 44–46
28. Brünger, A. T., Kuriyan, J., and Karplus, M. (1987) *Science* **235,** 458–460
29. Konnert, J. H., and Hendrickson, W. A. (1980) *Acta Crystallogr. Sect. A* **36,** 344–350
30. Brünger, A. T., Adams, P. D., Clore, G. M., DeLano, W. L., Gros, P., Grosse-Kunstleve, R. W., Jiang, J. S., Kuszewski, J., Nilges, M., Pannu, N. S., Read, R. J., Rice, L. M., Simonson, T., and Warren, G. L. (1998) *Acta Crystallogr. Sect. D Biol. Crystallogr.* **54,** 905–921
31. Brünger, A. T. (1992) *Nature* **355,** 472–475
32. Sheldrick, G. M., and Schneider, T. R. (1997) *Methods Enzymol.* **277,** 319–343
33. Ramachandran, G. N., Ramakrishnan, C., and Sasisekharan, V. (1963) *J. Mol. Biol.* **7,** 95–99
34. Holm, L., and Sander, C. (1993) *J. Mol. Biol.* **233,** 123–138
35. Maignan, S., Guilloteau, J. P., Fromage, N., Arnoux, B., Becquart, J., and Ducruix, A. (1995) *Science* **268,** 291–293
36. Eck, M. J., Atwell, S. K., Shoelson, S. E., and Harrison, S. C. (1994) *Nature* **368,** 764–769
37. Xu, W., Harrison, S. C., and Eck, M. J. (1997) *Nature* **385,** 595–602
38. Hof, P., Pluskey, S., Dhe-Paganon, S., Eck, M. J., and Shoelson, S. E. (1998) *Cell* **92,** 441–450
39. Poy, F., Yaffe, M. B., Sayos, J., Saxena, K., Morra, M., Sumegi, J., Cantley, L. C., Terhorst, C., and Eck, M. J. (1999) *Mol. Cell* **4,** 555–561
40. Pascal, S. M., Singer, A. U., Gish, G., Yamazaki, T., Shoelson, S. E., Pawson, T., Kay, L. E., and Forman-Kay, J. D. (1994) *Cell* **77,** 461–472
41. Gallagher, T., Gilliland, G., Wang, L., and Bryan, P. (1995) *Structure* **3,** 907–914
42. Bryan, P., Wang, L., Hoskins, J., Ruvinov, S., Strausberg, S., Alexander, P., Almog, O., Gilliland, G., and Gallagher, T. (1995) *Biochemistry* **34,** 10310–10318
43. Siegbahn, P. E. (2003) *J. Biol. Inorg. Chem.* **8,** 567–576
44. Rodriguez-Lopez, J. N., Tudela, J., Varon, R., Garcia-Carmona, F., and Garcia-Canovas, F. (1992) *J. Biol. Chem.* **267,** 3801–3810
45. Lerch, K. (1982) *J. Biol. Chem.* **257,** 6414–6419
46. Wichers, H. J., Recourt, K., Hendriks, M., Ebbelaar, C. E., Biancone, G., Hoeberichts, F. A., Mooibroek, H., and Soler-Rivas, C. (2003) *Appl. Microbiol. Biotechnol.* **61,** 336–341
47. Engh, R. A., and Huber, R. (1991) *Acta Crystallogr. Sect. A* **47,** 392–400